communications materials

ARTICLE

https://doi.org/10.1038/s43246-022-00248-0 OPEN

Controlling triplet–triplet upconversion and singlet-triplet annihilation in organic light-emitting diodes for injection lasing

Atul Shukla[1,2]✉, Monirul Hasan[1,2], Gangadhar Banappanavar[3], Viqar Ahmad[1,2], Jan Sobus[1,2], Evan G. Moore[4], Dinesh Kabra[3]✉, Shih-Chun Lo[1,4]✉ & Ebinazar B. Namdas[1,2]✉

Significant progress has recently been made in the field of organic solid-state lasers. However, achieving lasing action from organic semiconductors under electrical excitation remains challenging due to losses introduced by triplet excitons. Here, we report experimental and theoretical results that confirm a positive contribution of triplet excitons for electrically-driven organic lasing via a bimolecular triplet-triplet upconversion (TTU) mechanism. We study a model fluorescent material, 9-(9-phenylcarbazole-3-yl)-10-(naphthalene-1-yl)anthracene, revealing that TTU can lower the threshold current densities required to achieve lasing under current injection. However, to achieve the best performance, the singlet-triplet annihilation (STA) must be simultaneously minimized. Hence, an experimental strategy to simultaneously obtain high TTU with low STA is demonstrated in host-guest system with coumarin 545T as the guest laser dye. This system has a low amplified spontaneous emission threshold of 1.7 μJ cm^{-2} under nanosecond optical pumping, and a more than three orders of magnitude improvement in J_{50} in organic light-emitting diodes as compared to a reference blend.

[1] Centre for Organic Photonics & Electronics, The University of Queensland, Brisbane, QLD 4072, Australia. [2] School of Mathematics and Physics, The University of Queensland, Brisbane, QLD 4072, Australia. [3] Department of Physics, Indian Institute of Technology Bombay, Mumbai 400076, India. [4] School of Chemistry and Molecular Biosciences, The University of Queensland, Brisbane, QLD 4072, Australia. ✉email: a.shukla@uq.edu.au; dkabra@iitb.ac.in; s.lo@uq.edu.au; e.namdas@uq.edu.au

In recent years, organic solid-state lasers (OSSLs) have garnered significant attention because of their ability to provide tunable, coherent light emission while allowing compatibility with a variety of substrates such as silicon, glass, or plastic at low-cost processing techniques. Currently, most of the OSSLs are optically pumped using a pulsed excitation source with pulse widths ranging from femtoseconds (fs) to a few nanoseconds (ns)[1–6]. However, lasing from OSSLs under electrical excitation is expected to open new prospects for next-generation display, biomedical sensor, and lighting applications with unprecedented color purity[7–12]. These lasers can seamlessly integrate with existing manufacturing ecosystem such as Complementary metal-oxide-semiconductor (CMOS), organic light-emitting diode (OLED) display, and printing technologies. Interestingly, Sandanayaka et al. recently demonstrated indication of lasing emission under electrical pumping using 4,4′-bis[(*N*-carbazole)styryl] biphenyl (BSBCz) as the organic laser gain medium[13]. However, the devices demonstrated in the study were found to be unstable due to the high driving voltages required to achieve lasing emission. Hence, further studies towards the development of new materials for electrically pumped organic lasers with reduced threshold current densities are much required.

Achieving lasing emission under electrical excitation is a difficult task. This is primarily because of the trade-off in photoluminescence quantum yields (PLQYs) and charge carrier mobility of organic materials[14]. Obtaining high mobility in organic compounds essentially requires higher degree of π-π stacking between the chromophores in films, which in general, leads to drastic reduction in thin film PLQYs due to aggregate induced luminescence quenching[15]. To overcome this, molecular doping approach has been employed to achieve high film PLQYs, low lasing thresholds (E_{th}) in the case of optically pumped laser and high efficiency in OLED[16]. However, such doping approaches often lead to a reduction in charge carrier mobility of these systems[17]. Apart from the high mobility and high PLQY, organic laser gain medium should also possess a high radiative rate constant (k_r) and high electroluminescence (EL) quantum yield to achieve lasing action at low optical pump intensities and hence at low injection current densities[18]. To address these issues, continuous efforts are made to obtain high EL efficiencies from non-doped emitters with high k_r[19–22]. Unfortunately, the maximum internal quantum efficiency (IQE) of OLEDs based on fluorescent materials is only limited to 25%. On the other hand, OLEDs based on phosphorescent and recently developed materials exhibiting thermally activated delayed fluorescence (TADF)[5, 23, 24] provide 100% IQEs. However, these materials do not give stimulated emission due to their long excited-state lifetimes and/or low radiative rates. Hence, it is crucial to discover new classes of light-emitting materials that can possess high k_r and high EL quantum yields to achieve lasing action from organic semiconductors at low current densities. Anthracene derivatives have been one of the most extensively studied materials, which show efficient EL and high charge transport properties in non-doped OLEDs[15, 25–28]. Anthracene derivatives in OLEDs have continuously shown high external quantum efficiencies (EQEs), exceeding the theoretical limit of traditional fluorescent emitters for past several years[27–34]. This is mostly attributed to the high efficiency of triplet–triplet upconversion (TTU) in these anthracene derivatives. Recently Adachi et al. reported enhancement in TTU efficiency of anthracene derivatives close to 50% through spin-orbit coupling leading to high IQEs of close to 60%[35]. As evidenced through previous numerical simulations, the TTU enhanced device efficiency can be a promising route towards injection lasing[36]. However, reports highlighting the influence of TTU in OSSLs are very limited.

Apart from the issues highlighted earlier, fluorescent emitters also suffer from detrimental loss of radiative singlet excitons due to bimolecular processes such as singlet-triplet annihilation (STA) and singlet-polaron annihilation (SPA) under high current densities[36, 37]. Other loss mechanisms also include electric field-induced quenching and singlet-heat quenching (joule heating)[38]. Among all of the above-listed loss processes, STA has been shown to be the dominant loss mechanism under high current densities[37]. This is mainly due to long-lifetime and high generation yield of triplet excitons under electrical pumping leading to the accumulation of triplet excitons. Hence, while studying the impact of TTU, the critical role of STA should also be considered as the interplay between the two will determine the overall performance of the material.

In this work, we investigate the EL and light amplification properties of a model anthracene derivative 9-(9-phenylcarbazole-3-yl)-10(naphthalene-1-yl) anthracene (PCAN) with the chemical structure shown in Fig. 1a[32, 39–41]. The performance of PCAN-based OLEDs in neat and doped conditions was studied under steady-state and nanosecond pulsed excitation. We found that high EQEs of this material in non-doped conditions can be attributed to TTU at low current densities (J) while at higher current densities singlet-triplet annihilation (STA) becomes a detrimental factor leading to sharp EQE roll-off at high current densities. Time-resolved photoluminescence (TRPL) and transient absorption spectroscopy (ns-TAS) were performed to obtain further evidence of TTU and STA. The TTU and STA rate constants were then extracted through theoretical modeling of transient EL signals. The amplified spontaneous emission (ASE) characteristics of doped and neat films of PCAN under nanosecond-optical excitation coupled with exciton-exciton annihilation parameters were used to calculate the threshold current density (J_{th}) required to achieve population inversion under electrical pumping. The simulated J_{th} values show a clear reduction with increasing TTU rate constant. The numerical simulations also highlighted that STA rate constants need to be significantly reduced alongside increment in TTU rate constants to obtain net reduction in threshold current densities. An approach to obtain efficient TTU along with simultaneous reduction in STA is experimentally demonstrated through TTU-assisted host–guest system using high performing laser dye coumarin 545T (C545T) as dopant in PCAN. The molecular doping

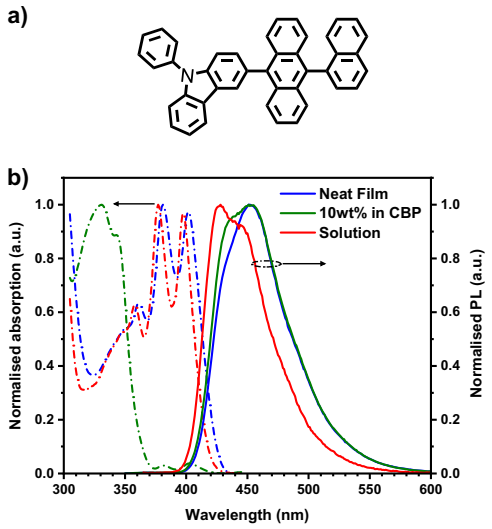

Fig. 1 Chemical structure, absorption and PL spectra of PCAN. a Chemical structure of PCAN. **b** Normalised absorption (dashed lines) and PL (solid lines) spectra of PCAN in toluene solution (red), neat film (green) and 10 wt% doped in CBP host matrix (blue).

of C545T in PCAN and CBP provided comparable ASE thresholds (1.7 and 1.6 μJ cm^{-2}, respectively) under ns-optical excitation. However, transient and steady-state EL measurements showed over 3 orders of magnitude improvement in J_{50} (current density at which EQE is declined by half from its maximum value) in PCAN-host-based OLEDs as compared to reference devices fabricated from CBP host. To the best of our knowledge, this is the first comprehensive study on TTU material involving both experimental and theoretical studies that sheds light on the interplay between triplet upconversion, singlet-triplet annihilation, and lasing threshold.

Results and discussion

Steady-state photophysical properties. Photophysical properties of PCAN were studied in toluene solution, neat, and doped films [10 wt% PCAN in 4,4′-bis(*N*-carbazolyl)-1,1′-biphenyl (CBP)]. Figure 1b shows the normalised absorption and photoluminescence (PL) spectra of PCAN in dilute toluene solution, neat and doped films. The absorption spectra of PCAN in solution and neat films show typical vibronic structures, arisen from the anthracene unit while absorption spectra in the doped film are dominated by CBP. The solution PL spectrum of PCAN shows a major emission peak at 428 nm along with a shoulder at 445 nm. On the other hand, neat film PL spectrum was found to be red-shifted with emission peak at 452 nm, compared to that of solution. The red shift in emission can be attributed to the intermolecular interaction in neat films, which is absent in dilute solutions. The emission spectra in doped films also showed a major peak at 452 nm, though the contribution of shoulder at 435 nm was found to be enhanced in doped films, suggesting that the intermolecular interaction in doped films is significantly reduced as compared to those of neat films. The above PL features are further supported by the PLQY values. The PLQY of dilute toluene solution was found to be 64 ± 7%, while for neat films this value dropped to 37 ± 6%. However, doping in CBP host helps retain the high PLQY value of 54 ± 6% for this system.

OLED characteristics. To understand the EL properties, we fabricated OLEDs with non-doped and 10 wt% PCAN doped in CBP host as the emissive layers (EMLs). The structure of the fabricated OLEDs consisted of indium tin oxide (ITO)/PEDOT:PSS (40 nm)/NPB (20 nm)/EML (40 nm)/Alq_3 (20 nm) /LiF (0.8 nm)/Al (100 nm), where PEDOT:PSS = poly(3,4-ethylenedioxythiophene): poly(styrenesulfonate), NPB = *N*,*N*-bis(naphthalene-1-yl)-*N*,*N*-bis(phenyl)benzidine, Alq_3 = tris(8-hydroxy-quinolinato)aluminum. To obtain better electron injection in the doped devices 1,3,5-tris(1-phenyl-1*H*-benzimidazol-2-yl)benzene (TPBi) was used as the electron transport layer instead of Alq_3.

Figure 2a shows device EQEs as a function of current densities for neat and doped films. OLEDs based on doped films showed sharp EQE roll-off with increasing current densities while non-doped devices showed a "roll-up" in EQE with increasing current densities till ≈20 mA cm^{-2}. The current density and luminance *versus* voltage (*J*–*V*–*L*) characteristics, and EL spectra of PCAN-based doped and non-doped OLEDs are shown in Supplementary Fig. 1a–c. Supplementary Table 1 shows the performance comparison of PCAN-based doped and non-doped devices. Even though the peak EQE of 2.8% at 1600 cd m^{-2} achieved in this study for non-doped devices was found to be slightly lower than previous reports of PCAN[32], it is interesting to note that peak EQE still exceeds the theoretical EQE limit of ≈1.9% for typical fluorescent OLEDs (calculated from the neat-film PLQY of 37%, assuming singlet: triplet generation of 1:3 and light out-coupling of 20%). Devices with doped PCAN EMLs on the other hand

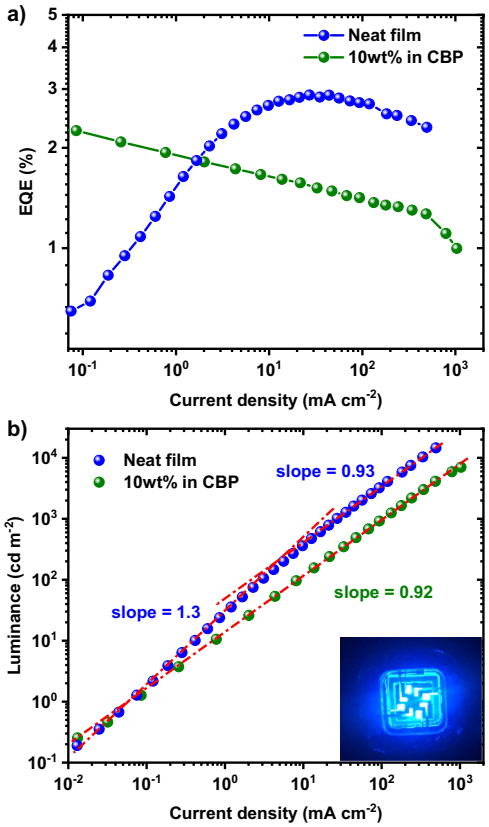

Fig. 2 Performance characteristics of doped and non-doped PCAN-based OLEDs. a EQE vs current density and (**b**) Luminance vs current density characteristics for OLEDs based on doped (green) and non-doped (blue) PCAN EMLs (Inset: Image of the EL from non-doped PCAN-based OLEDs operated at 8 V).

showed a peak EQE of ≈2.3% at 1 cd m^{-2}, which is lower than that achieved with non-doped devices and the theoretical fluorescent limit (≈2.75%) even despite the doped EML having a higher PLQY (≈55%). These results suggest a vital contribution of triplet to singlet upconversion in non-doped devices, which is otherwise absent or significantly reduced in doped devices, leading to the superior performance of non-doped PCAN OLEDs. Furthermore, the absence of any strong donor-acceptor moieties in the molecular structure dismisses the presence of TADF or "hot exciton" channel, which can be mediated via hybrid charge transfer-locally excited (HLCT) characters of singlet and higher lying triplet states[35, 42, 43].

Figure 2b shows the comparison of luminance *versus* current density plots (log-log scale) for doped and non-doped devices. Herein, doped devices showed characteristics typical to fluorescent OLEDs with a slope close to 1. This suggested a linear relationship between output photons and excitons generated. Non-doped devices on the other hand showed two regimes with a slope of ≈1.3 under low current densities and a slope of ≈1 when current densities are increased. As seen in previous studies, this non-linear relationship (slope > 1 in log–log plots) between luminance and current density is typically suggestive of the TTU process[44].

TRPL and fluence dependent measurements. To obtain insights into the non-linear relationship (slope > 1) between luminance and current density in PCAN neat-film devices, we studied time-resolved characteristics of PCAN under optical excitation. Supplementary Fig. 2 shows the time-correlated single-photon

counting (TCSPC) decay curves at peak PL wavelengths for PCAN in dilute toluene solution, neat and 10 wt% doped in CBP films. In dilute toluene solution (deoxygenated), the fluorescence intensity decayed mono-exponentially with lifetime of 3.5 ns. However, the neat and doped films showed bi-exponential decay in prompt fluorescence (PF) along with small contributions from delayed fluorescence (DF) in the longer time domains. The details of the lifetime and their respective contributions are listed in Supplementary Table 2. For neat films, the fast components of 1.1 ns (81%) and 3.5 ns (14%) in the PF can be attributed to aggregates and non-aggregate states respectively. While the presence of long-lived (≈85 ns) DF is a characteristic feature observed in the case of upconversion of triplet excitons to singlet excited-states via TTU process[45]. The low contribution from DF can be attributed to a low triplet yield (due to a low intersystem crossing rate) in anthracene derivatives as reported in previous studies[46] and also to the low excitation power of the TCSPC system.

To further study the long-lived DF in neat and doped films, we used variable gate delays (ranging from picosecond to microsecond range) based TRPL technique. Supplementary Fig. 3a shows the complete PL decay kinetics of the neat and doped films excited at 355 nm (840 ps pulse width) laser source with excitation fluence of 80 μJ cm^{-2}. The neat films show distinct long-lived DF, compared to the doped films. Interestingly, neat films showed two DF regions with lifetime in order of several hundreds of ns (black line) and 10 μs (magenta line), respectively. We attribute the origin of the two DFs in neat films to different triplet diffusivity due to different orientations of chromophores in the bulk. A similar impact of molecular packing on DF has been previously observed for several systems[47]. Supplementary Fig. 3b shows the PL spectra for neat films at different gate delays. The similarity in spectra for PF and DF confirms that both emissions arise from the same excited-state species.

While the non-linear dependence of steady-state emission as a function of excitation intensity can be clearly seen under electrical excitation in the previous section, optical excitation with different laser fluence did not show such non-linear behaviors. This can be simply attributed to lower contributions of DF due to a much lower triplet population under optical pumping as compared to that in electrical pumping where triplet density is significantly higher. Hence, to obtain an indication of TTU under optical excitation in the neat films, we carried out time-resolved fluence-dependent PL studies and carefully monitored the relative contribution of DF and PF. Supplementary Fig. 3c shows normalised DF intensities as a function of normalised PF intensities at the same pump fluence. Herein, the absolute PF and DF intensities were obtained by integrating the respective spectra over all wavelengths. We note that under lower fluence regions, both PF and DF follow almost linear relationship and then start to shift towards almost quadratic relation at higher pump fluence. This can be attributed to increment in triplet excited-state population with increasing fluence leading to enhancement in contributions arisen due to TTU. The near quadratic relation in fluence-dependent studies confirmed the presence of TTU, which is consistent with non-linear relation of luminance and current density under electrical excitation.

To further confirm TTU under optical excitation, triplet photosensitization studies were performed with platinum(II) octaethylporphyrin (PtOEP) as a triplet sensitizer[48]. The schematic of the triplet sensitized TTU process is shown in Supplementary Fig. 4, while the detailed experimental methods and steady-state photophysics discussed in Supplementary Note 1 and Supplementary Fig. 5, respectively. Figure 3a shows the spectral evolution of PCAN (10^{-2} M) + PtOEP (10^{-5} M) solutions as a function of increasing pump power. The intensity at 448 nm (corresponding to upconverted singlet emission of PCAN) as a function of pump fluence is further shown in Fig. 3b. The upconverted singlet emission intensity was found to follow a non-linear relationship with pump power with slope >1 in the entire measurement range. At low power density, the output emission in the blue region was found to have a clear quadratic relation, which then saturates at higher power densities due to other bimolecular annihilation processes. The intensity *versus* fluence plot for other transition is shown in Fig. 3c. While the intensities for all the other signals followed a near linear dependence with pump fluence, the phosphorescence emission of PCAN was found to have slope <1. This substantiates the presence of TTU in PCAN, which further explains the non-linear relationship (slope >1) between luminance and current density in the neat-film devices. Figure 3d shows the image of PCAN (10^{-2} M) + PtOEP (10^{-5} M) under 532 nm laser excitation. The fact that we did not observe any light emission from solution with only PCAN (10^{-2} M) when excited at 532 nm, suggested that photon upconversion observed in PCAN (10^{-2} M) + PtOEP (10^{-5} M) solution proceeds only via TTU and not through the non-linear two-photon absorption process.

Nanosecond transient electroluminescence studies. To obtain a complete picture of TTU that contributed to the EQE "roll-up" processes, we studied the transient electroluminescence at high current densities. The OLEDs were subjected to 100 ns electrical pulse at high current density. The prime benefit of applying a short pulse to the OLED is the suppression of the joule heating. The schematic of the transient EL setup is shown in Supplementary Fig. 6. The device areas of the OLEDs were reduced to 0.3 mm^2 to minimize the RC response distortion by reducing the geometrical capacitance. Supplementary Fig. 7a, b shows the transient current density and EL intensity in non-doped and doped PCAN-based OLEDs, respectively (under 100 ns voltage pulse). Contrary to DC results in the "OLED characteristics", where the operation of OLEDs is limited to low current densities (<1 A cm^{-2}), higher current densities (>2.6 A cm^{-2}) were used under pulsed excitation. The current response of both doped and non-doped OLED shows sharp rise (typical response under space charge limited current (SCLC) conditions) and reaches steady-state after 15 ns (Supplementary Fig. 7). Figure 4a, b depicts the normalised EL transients for non-doped and doped devices, respectively, at both 20 and 40 V. For non-doped devices at 20 V, EL intensity shows a sharp rise after 25 ns, followed by gradual increment as the time progresses while at 40 V, EL intensity peaks and then rapidly reduces to 73% of the initial intensity. The EL intensity here is a representative of the singlet excitons, the gradual rise with time in EL intensity at 20 V indicates the triplet to singlet upconversion due to TTU, while the rapid reduction of intensity at 40 V is a signature of dominating STA, leading to a reduction in singlet density. STA primarily takes place via Förster resonance energy transfer (FRET), whose efficacy is determined by the spectral overlap between PL and triplet excited-state absorption ($T_1 \rightarrow T_n$) bands.

To confirm STA in PCAN, we performed nanosecond transient optical pump-probe absorption spectroscopy. Supplementary Fig. 8 shows the triplet and singlet excited-state absorptions for neat PCAN films measured under vacuum. The long-lived triplet excited-state absorption band positioned between 400 and 500 nm was found to overlap strongly with the PL, confirming the strong influence of STA in PCAN. Supplementary Fig. 9 further shows the normalised EL turn-off characteristics for doped and non-doped devices at 20 V, showing prompt and delayed components.

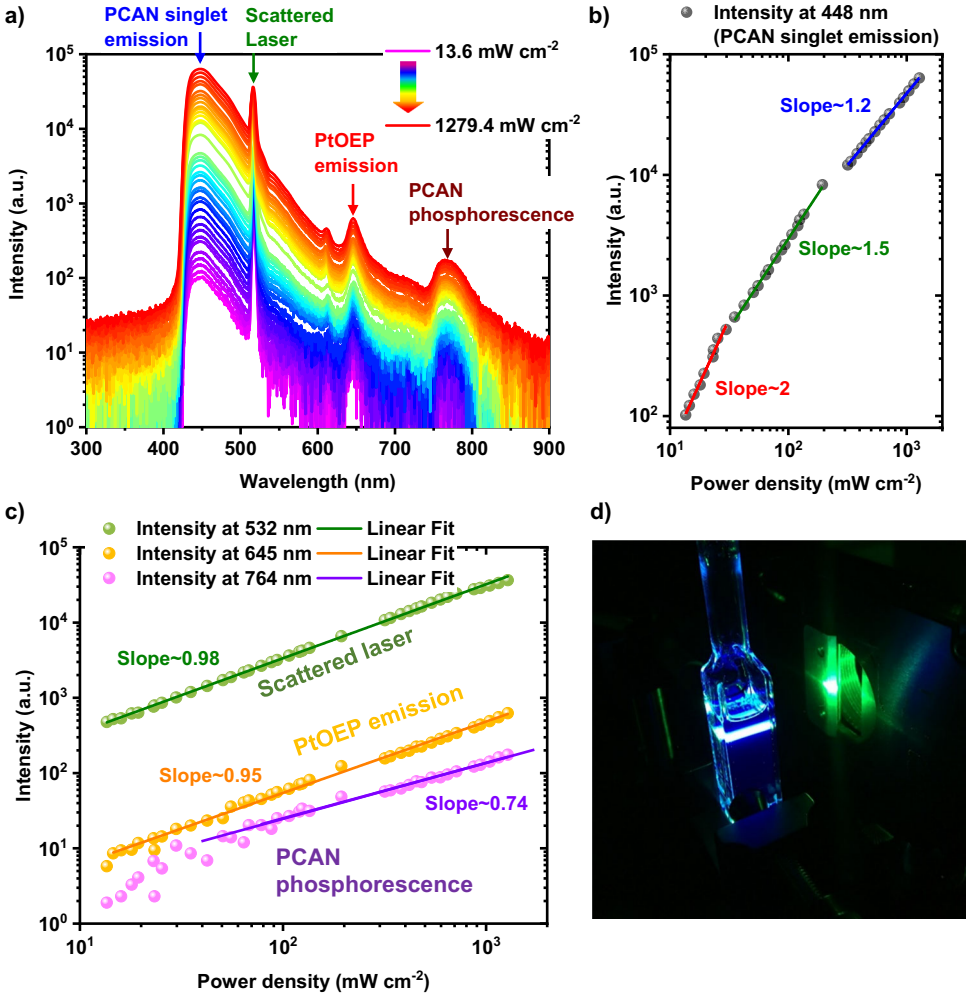

Fig. 3 TTU in PCAN through triplet photosensitization. a Spectral evolution as a function of pump power in PtOEP (10^{-5} M) + PCAN (10^{-2} M) solution. **b** Intensity vs power density plot for upconverted singlet emission of PCAN and (**c**) evolution of intensity with fluence for all the other transition observed in (**a**). **d** Image of PtOEP (10^{-5} M) + PCAN (10^{-2} M) in toluene solution under illumination with 532 nm laser source.

Next, we quantitatively extracted the STA and TTU rate constants from singlet and triplet populations using rate equations designed for anthracene derivatives (details in Supplementary Note 2). Figure 5a, b shows the theoretical fits and the corresponding triplet population density for non-doped and doped devices, respectively at 20 and 40 V. From EL transients, STA and TTU rate constants for doped devices are obtained as 1.44×10^{-9} and 6.67×10^{-11} cm^3 s^{-1}, respectively (Supplementary Table 4). The extracted annihilation rate constants for non-doped PCAN devices are significantly higher than the doped PCAN devices with a value of 7.37×10^{-9} cm^3 s^{-1} for STA and 2.32×10^{-10} cm^3 s^{-1} for TTU (Supplementary Table 3). These rate constants are well within the typical range of STA and TTU rate constants reported for organic semiconductors in literature[49]. Clearly, the STA rate constant for the non-doped devices is much higher than typical fluorescent OLED emitters but this is still lower than those reported for anthracene single crystals[50]. The higher value of TTU rate constant in non-doped devices explains the higher peak EQEs, compared to doped devices at steady-state condition as contribution from delayed fluorescence is significantly enhanced. However, the higher STA rate constant in non-doped devices implies a trade-off between TTU and STA[47, 51–54]. Furthermore, it is interesting to note that there is appreciable TTU in doped devices, which signifies the presence of intermolecular interactions even under 10 wt% doping of PCAN. Similar effects have been previously demonstrated in other host–guest systems as well[26, 27].

Implications of TTU on threshold current densities. To study the light amplification properties of PCAN, we explored the ASE characteristics for PCAN neat and doped films. The ASE threshold (E_{th}) was obtained from the abrupt change of slope in plots of output intensity from the edge of the sample *versus* input excitation fluence along with a drop in full width at half maxima (FWHM) of the output spectra. Supplementary Fig. 10a, b shows the typical input–output–FWHM plots and emission spectra at various intensities for neat and doped films, respectively. The ASE threshold for doped and neat films were 16 μJ cm^{-2} and 500 μJ cm^{-2} respectively. The light amplification in the TTU-based emitter is very encouraging. However, the key question is whether TTU-based material is beneficial under electrical injection, a critical figure of merit for the development of electrically pumped organic lasers.

The ASE threshold measured above can be translated into threshold singlet exciton density by employing optical model as described in Supplementary Note 3. The threshold singlet exciton density was found to be 3×10^{19} cm^{-3} and 1×10^{18} cm^{-3} for neat and doped films, respectively. We then extracted the threshold current density (J_{th}) required to reach this singlet exciton density

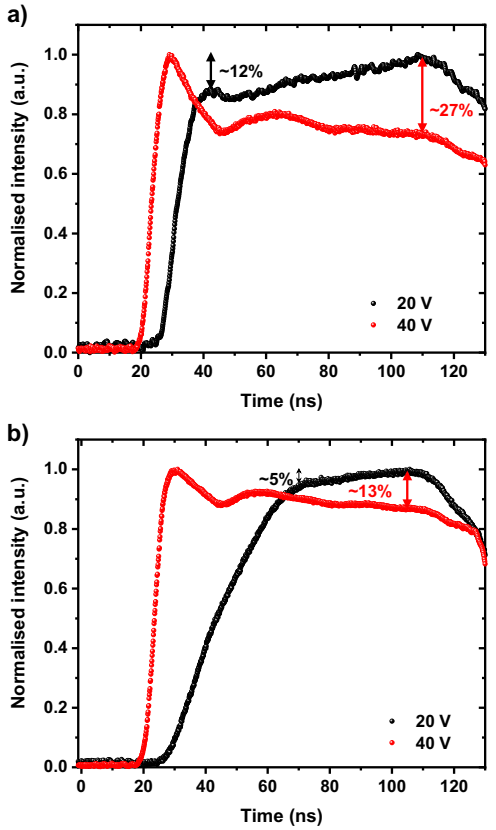

Fig. 4 Time-resolved EL response of doped and non-doped OLEDs. Transient EL response of (**a**) non-doped and (**b**) doped PCAN-based OLEDs at bias of 20 V (black) and 40 V (red).

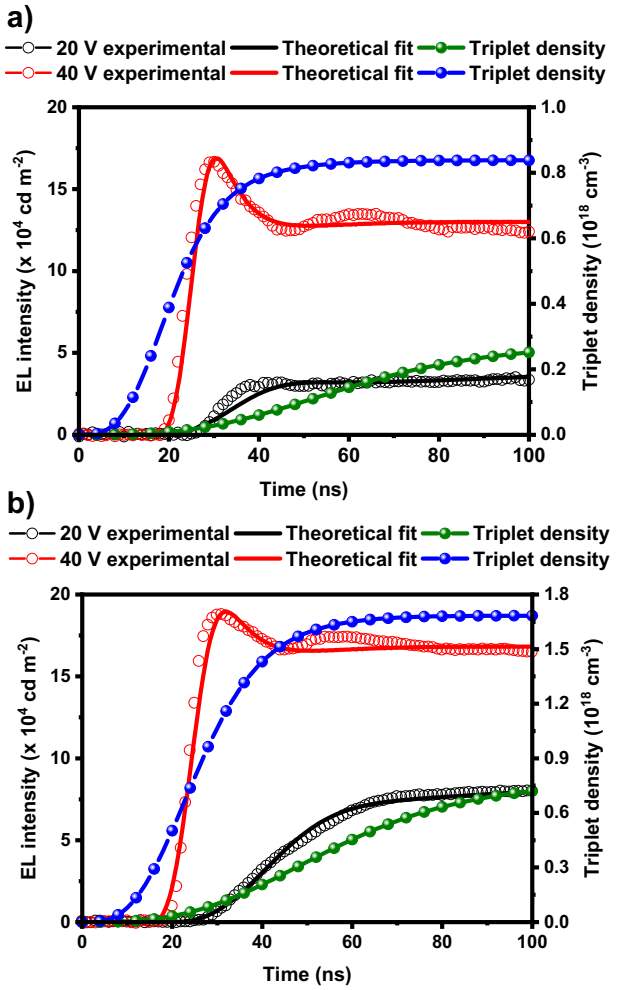

Fig. 5 Simulation of EL response under pulsed electrical excitation. Experimental EL intensities overlapped with the theoretical fits and the corresponding triplet density extracted from the model for (**a**) non-doped and (**b**) doped PCAN-based OLED at 20 (black) and 40 V (red).

under electrical excitation. For comparative analysis, we considered three conditions: (1) an ideal case with no annihilation of singlet-singlet (SSA), singlet-triplet (STA), and triplet-triplet (TTU) excitons; (2) when only STA and (3) when both STA and TTU are taken in account. Using the k_{STA} and k_{TTU} values extracted in the section "Nanosecond transient electroluminescence studies", we calculated the singlet exciton density as the function of current density in all three conditions. Figure 6a, b shows the calculated singlet exciton density as the function of current density for doped and neat systems, respectively. The threshold singlet exciton density required for lasing is shown by the horizontal blue line. It is interesting to note that when only STA is considered, the singlet population does not reach the threshold required to achieve lasing in both doped and non-doped systems. This suggests that the losses due to STA are extremely detrimental to lasing. When both STA and TTU rate constants are considered, the singlet population can reach the threshold of current density, $J_{th} \approx 40$ kA cm^{-2} for doped devices. While these results clearly highlight the positive impact of TTU on reducing the J_{th} required to achieve injection lasing in organic semiconductors, it is important to mention that in this study we are primarily limited by intrinsic light amplification properties of PCAN in this case. The optical pumping thresholds achieved for both neat and blend films are extremely high for the standard of electrically pumped lasers[3, 6, 13] (typically requires $E_{th} < 2$ μJ cm^{-2}).

To further elucidate the impact of STA and TTU on lasing thresholds, we varied k_{TTU} in the range of 10^{-11}–10^{-10} and k_{STA} in the range of 10^{-9}–10^{-8} and simulated the J_{th} in doped PCAN system while keeping the other rate constants unchanged. Figure 7 shows the simulated values of J_{th} as a function of k_{TTU} and k_{STA} values. As k_{TTU} is increased, J_{th} reduces gradually. In contrast, J_{th} increases rapidly as k_{STA} increases. A comparison of J_{th} values as a function of linear increase in k_{TTA} and k_{STA} is further depicted in Supplementary Fig. 11. Clearly, the STA has much severe detrimental impact on J_{th}, whereas TTU facilitates in reducing the lasing threshold. It is important to note that TTU proceeds via Dexter energy transfer (DET), while STA predominantly takes place via Förster-type energy transfer mechanism. The rate of STA largely depends on the overlap between the triplet excited-state absorption and emission spectra. Hence, having separation between triplet absorption and singlet emission can typically reduce the STA while maintaining the high TTU yields.

TTU in host–guest system. While the inferences drawn from numerical simulations are encouraging, the performance of the neat PCAN is clearly limited by its poor light amplification properties and high STA rates. To further overcome these factors, we used a host–guest system with PCAN as the host and Coumarin 545T (C545T) as the guest emitter. The singlet and triplet energy levels of C545T were found to be 2.5 eV and 2.0 eV respectively[55]. Hence, the singlet excitons generated on PCAN can be transferred to C545T via FRET, while triplets of C545T are quenched by DET due to low-lying triplet energy level of PCAN. Furthermore, the accumulated triplet excitons in PCAN can be upconverted to singlet by TTU and transferred to singlet energy

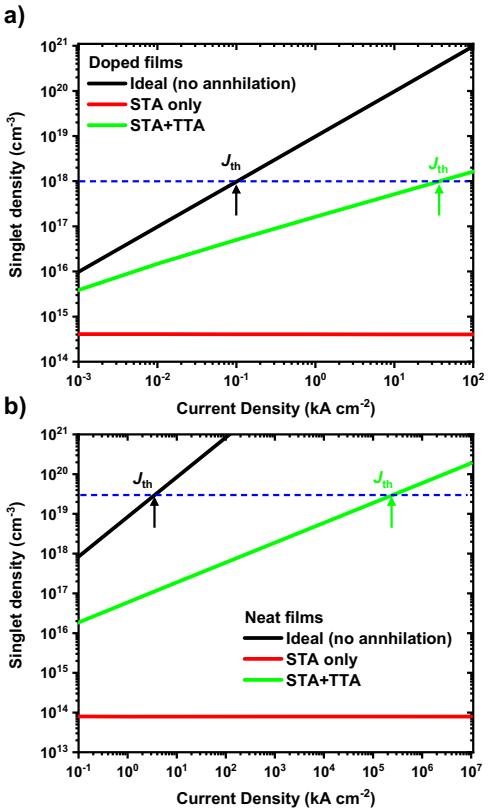

Fig. 6 Theoretical simulation of threshold current density required to reach lasing. Simulated singlet exciton density as a function of current densities in all three conditions for (**a**) doped and (**b**) non-doped devices with blue line representing the singlet density at ASE threshold.

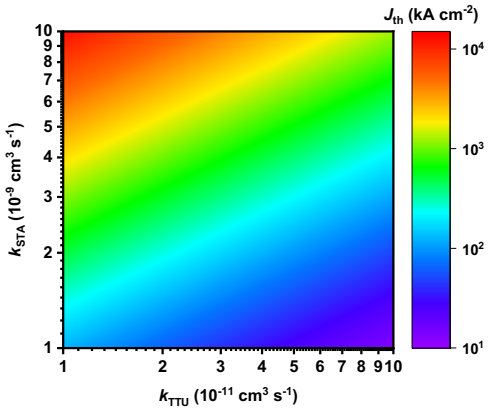

Fig. 7 Correlation between STA, TTU, and threshold current density. Variation of threshold current density as a function of STA and TTU rate constants.

level of C545T. The schematic representation of energy transfer and TTU process in this system is shown in Supplementary Fig. 12.

Photophysical properties of the C545T: PCAN blend were studied with variable doping ratio of C545T (1, 3, and 5 wt% C545T in PCAN). For better comparison, we also studied the photophysics of the same C545T doping in CBP host. In the case of C545T: CBP blend, both singlet and triplet excitons are confined on C545T due to high triplet energy level of CBP ($T_1 \approx 2.66$ eV)[5]. Supplementary Fig. 13 shows the absorption and emission spectra for different doping ratios of C545T in PCAN and CBP hosts with corresponding PLQY, and k_r values listed in Supplementary Table 5. The PLQY in both the hosts was found to be ≈90% for 1 wt% doping, followed by subsequent reduction in PLQY for higher loading of C545T due to aggregate induced quenching. The 1 wt% doping ratio was also found to exhibit the highest k_r value in both host matrices. Interestingly, the k_r values obtained for C545T-based host–guest system were found to be significantly larger as compared to those obtained in the case of neat and blend PCAN. Furthermore, in C545T: PCAN-based host–guest system, the triplet excitons are expected to predominantly accumulate in PCAN. Therefore, it is vital to have a good spectral separation between the triplet excited-state absorption of PCAN and singlet emission of C545T. Supplementary Fig. 14 shows the triplet absorption spectra (averaged from Supplementary Fig. 8) of PCAN overlapped with emission of PCAN neat film and C545T: PCAN (1:99 wt%) blend films. Clearly, the spectral overlap for C545T: PCAN (1:99 wt%) blend is significantly reduced as compared to that of neat PCAN, suggesting much required reduction in STA in this system.

Next, we examined the light amplification characteristics of C545T in PCAN and CBP hosts. Due to high k_r values, samples with 1 wt% doping of C545T were chosen for ASE measurements. The output intensity and FWHM vs input pump fluence along with spectral narrowing for both PCAN and CBP hosts are shown in Fig. 8a, b. The ASE thresholds obtained for both cases were found to be comparable. Furthermore, E_{th} <2 μJ cm^{-2} in both host matrices are significantly lower than those obtained in the section "Implications of TTU on threshold current densities" and are also comparable to previously reported thresholds with C545T[56]. These results highlight that high radiative rate is critical towards achieving population inversion at relatively low singlet exciton densities.

To show the positive impact of TTU on electrically pumped organic lasers, we fabricated solution-processed OLEDs with 1 wt % C545T doped in CBP and PCAN hosts as the EMLs. The structure of the fabricated OLEDs (see Supplementary Fig. 15a) consisted of indium tin oxide (ITO)/PEDOT: PSS (40 nm)/ EML (40 nm)/TPBi (60 nm) /LiF (0.8 nm)/Al (100 nm). The *J*–*V*–*L* characteristics of OLEDs with EMLs based on 1 wt% C545T doped in PCAN and CBP hosts are shown in Supplementary Fig. 15b, while the EQE as a function of current density is shown in Supplementary Fig. 15c. Interestingly, both OLEDs demonstrated peak EQEs of ≈3%; however, OLEDs based on CBP host exhibited strong EQE roll-off characteristics from very low current densities. This suggests presence of strong singlet quenching in this system from bimolecular processes such as SSA, SPA, and more dominantly from STA. Remarkably, OLED based on C545T: PCAN (1:99 wt%) EML showed negligible efficiency roll-off with EQE >3% even at high current density values of 100 mA cm^{-2}. This can be partially attributed to both reduced STA and efficient TTU in PCAN: C545T-based host–guest system. Also, it should be noted that peak EQE achieved in both the OLEDs are lower than the theoretical fluorescent limit (≈4.5%). This can be ascribed to poor charge balance in the solution-processed device architecture as compared to thermally evaporated OLEDs shown in the section of "OLED characteristics". Nevertheless, we performed transient EL studies for both OLEDs to get further understanding of the bimolecular process in both host–guest system.

Supplementary Fig. 16 shows the normalised transient EL response of OLEDs based on C545T: CBP (1:99 wt%) EML under variable voltage with pulse width ≈400 ns. The EL response was found to reach the maximum well within initial 100 ns, followed by a strong reduction in EL intensity. The reduction in EL intensity was found to be more severe under higher voltages, clearly indicating that EQE roll-off in Supplementary Fig. 15c in

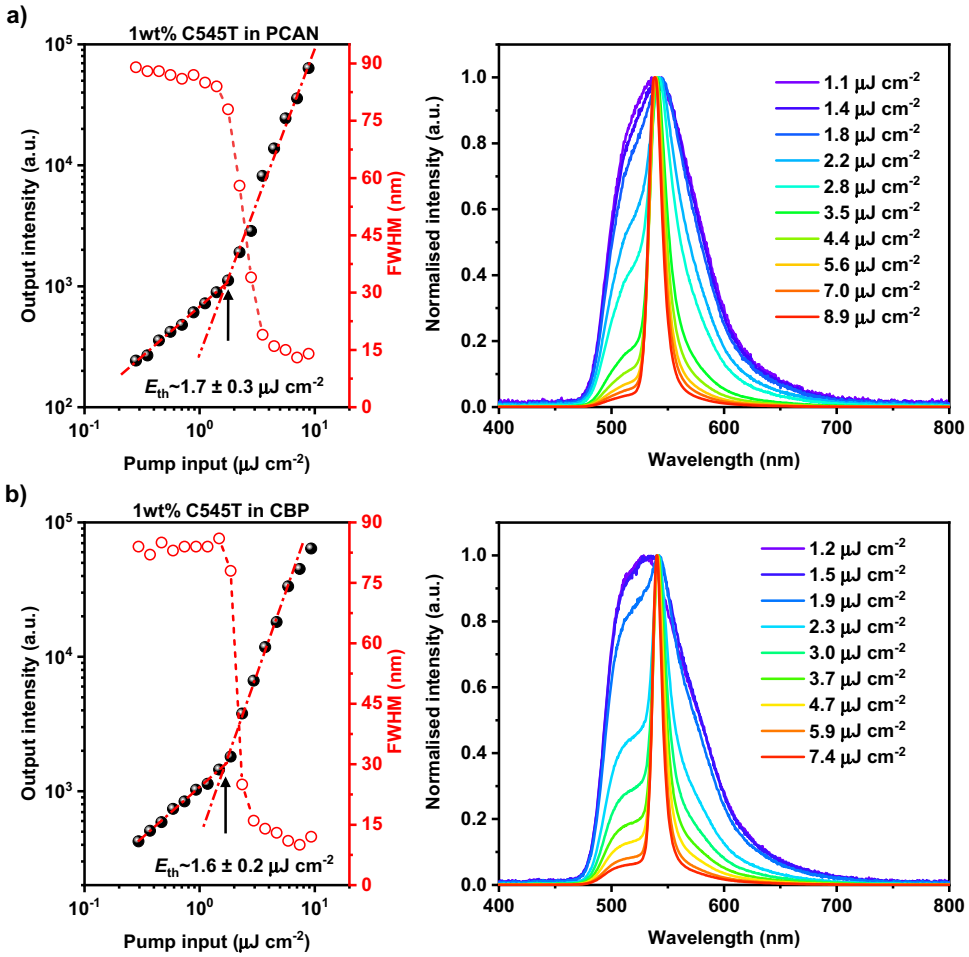

Fig. 8 Light amplification characteristics of 1 wt% C545T doped in PCAN and CBP hosts. Input–output–FWHM and spectral narrowing for blend films with 1 wt% C545T doped in (**a**) PCAN and (**b**) CBP hosts.

this system arises due to the dominance of STA. Supplementary Fig. 17 shows the absolute and normalised transient EL results for C545T: PCAN (1:99 wt%) OLEDs. Contrary to OLEDs with CBP host, EL intensity in C545T: PCAN system was found to reach the maximum value only at longer time domains (>1 μs) under electrical excitation. These results suggest a significant contribution in EL arising from triplet to singlet upconversion, similar to the one corroborated in neat PCAN OLEDs in the section "Nanosecond transient electroluminescence studies" and also reported previously for TADF assisted fluorescent systems[5]. Hence, we used longer pulse widths to study C545T:PCAN (1:99 wt%) based OLEDs. The width of the input voltage pulse was reduced from 8 μs to 4 μs at higher voltages to avoid device breakdown and reduce joule heating. Even under high current densities (≈35 A cm^{-2}), C545T:PCAN (1:99 wt%) based OLEDs demonstrated longer saturation time to attain maximum EL, this clearly suggest efficient TTU in this system along with a significant reduction in STA. Interestingly, time required for reach EL saturation was found to reduce with increasing voltages and can be attributed to the strong triplet quenching at higher voltages due to triplet-polaron (TPA) interactions[53].

Using peak luminance at EL saturation, we plotted the combined *J*–*V*–*L* and EQE *versus* current density response for the C545T: PCAN (1:99 wt%) OLED under DC and pulsed operation as shown in Fig. 9a, b, respectively. The peak current density and brightness achieved in this case were found to be ≈35 A cm^{-2} and ≈75 × 10^4 cd m^{-2} respectively. Furthermore, as shown in Fig. 9b, J_{50} (current density at which EQE is declined by half from its maximum value) in C545T:PCAN (1:99 wt%) OLED was found to be 3 orders of magnitude higher than that in C545T:CBP (1:99 wt%) OLED, highlighting clear experimental enhancement attained in device performance through improved TTU and reduced STA. It should also be noted that EQE roll-off in C545T:PCAN (1:99 wt%) OLED at current densities reported here may arise from combined contributions of (1) selective carrier trapping due to the use of multilayer OLED architecture[57], (2) joule heating due to comparatively longer pulse widths[58], (3) reduced charge balance in EML at higher current densities, and (4) exciton–polaron interactions[59]. Hence, further optimization of device structure is critical to overcome the above stated factors, however our results clearly substantiate positive contribution of TTU for electrically pumped organic lasers.

Conclusion

In summary, we report both experimental and theoretical results that confirm the positive contribution of TTU for the scope of electrically driven organic laser. We selected PCAN as a model material exhibiting efficient triplet–triplet upconversion and showed light amplification properties under optical pulse excitations. We studied the transient EL response of PCAN OLEDs and demonstrated that triplet population plays a critical role in controlling the device efficiency as a function of current density through TTU and STA processes. Furthermore, by theoretical modeling we showed that the threshold current densities required to achieve light amplification can be significantly reduced with

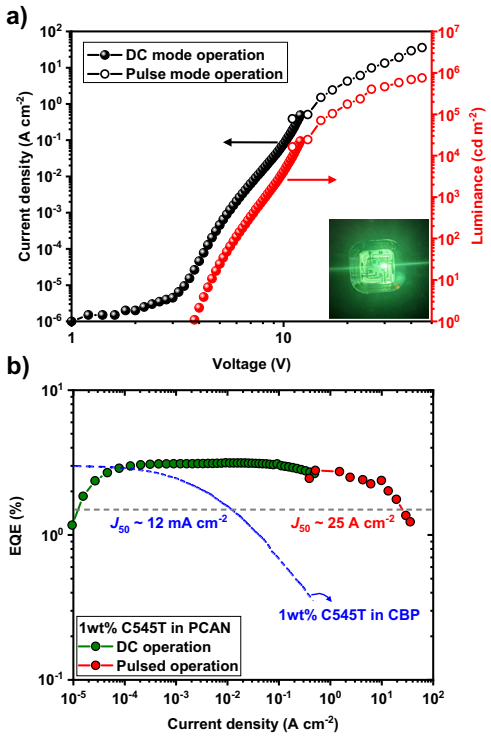

Fig. 9 DC and pulsed operation characteristics of C545T:PCAN (1:99 wt%) based OLEDs. a Combined *J–V–L* characteristics of C545T: PCAN-based OLEDs under DC pulsed operation. [Inset: Image of the EL from C545T: PCAN (1:99 wt%) OLEDs operated at 30 V]. **b** EQE *versus* current density comparison for OLEDs with 1 wt% C545T doped in CBP and PCAN hosts.

the aid of TTU. The results from theoretical modeling are further substantiated experimentally through TTU assisted host–guest system showing low ASE thresholds under optical pumping and efficient EL under high current injection. We believe these results are important for developing a new class of TTU-based laser materials for injection lasing.

Methods

Photophysical measurements. UV-visible absorption spectra for thin films and solutions were measured using Cary-5000 UV–Vis spectrometer. Horiba Jobin Yvon Fluoromax was used to measure PL spectra. Solution PLQYs were determined using Quinine sulfate in 0.1 M H_2SO_4 as the standard (PLQY = 55%) as the standard. Optical density of standard and the sample were measured to be 0.1 at excitation wavelength of 360 nm[57]. Solid-state PLQY measurements were performed using a calibrated integrating sphere[58]. Nanosecond transient absorption spectroscopy (TAS) were performed as described in the literature[10]. Pump wavelength of 400 nm was used to excite the sample. TCSPC measurements were performed using Halcyone fluorescence spectrometer with IRF (instrument response function) of 150 picoseconds (ps) with excitation wavelength 337 nm.

Thin-film preparation. Thin films for photophysical and ASE measurements were prepared using the same procedure. PCAN and C545T were purchased from LUMTEC and used as purchased. Non-doped and CBP doped films were deposited by thermal evaporation under high vacuum (10^{-6} mbar) on pre-cleaned fused silica substrates to obtain thin films with 200 nm thickness as measure by Dektak 150 profilometer (Bruker). All the substrates were cleaned using acetone, isopropanol followed by UV-ozone.

OLED fabrication and electrical characterization. OLED for DC and pulse measurements were fabricated on top of pre-patterned and cleaned ITO-glass substrates with ITO thickness of 100 nm. Substrates were cleaned by ultrasonication in de-ionized water with Alconox for 15 min, followed by ultrasonication in de-ionized water, acetone and isopropanol for 5 min each. A 40 nm thick PEDOT:PSS (Ossila AI 4083) layer was spin-coated on top of ITO and annealed at 150 °C for 20 min. NPB (20 nm), EML (40 nm), TPBi/Alq_3 (20 nm), LiF (0.8 nm), and Al (100 nm) layers were sequentially deposited by thermal evaporation under high vacuum (≈10^{-6} mbar). In solution-processed OLEDs, EML was spin-coated from 10 mg ml^{-1} toluene (for PCAN)/chloroform (for CBP) solutions at 3000 RPM to achieve thickness of 30–40 nm. The DC *J–V–L* characteristics of the OLEDs (area ≈ 4 mm^2) were measured inside nitrogen filled glovebox using a Keithley 2400 source meter and absolute EQE measurement setup (Hamamatsu photonics C9920-12) with a calibrated integrating sphere. Transient EL characteristics were measured by exciting the OLED devices (area ≈ 0.3 mm^2) using AVTECH pulse generator, AVX1011-B1-B, with rise and fall time of 2 ns. EL response was recorded with a calibrated photomultiplier tube (Hamamatsu, H10721–20), connected to a digital oscilloscope (Teledyne LeCroy, 2 GHz). Brightness was calculated using emission spectrum of the devices and taking in account calibration factor for the photomultiplier tube (assuming Lambertian emission).

TRPL measurements. For the time-resolved spectroscopy the neat and doped films were mounted in the vacuum chamber with low pressure in the order of 10^{-5} mbar. Samples were excited at 355 nm using Nd: YAG INNOLAS LASER operating at 1 kHz repetition rate with 840 ps pulse width. Highly sensitive gated iStar Andor ICCD was used to collect the prompt and delayed emission.

Triplet photosensitization measurements. The triplet photosensitization experiments were performed in degassed toluene solutions. PtOEP was purchased from Sigma-Aldrich and used without further purification. Samples were degassed using the freeze-pump-thaw method. For the fluence-dependent measurements, samples were excited using a CW laser with emission wavelength 532 nm. The excitation beam was focused into a rectangular spot with dimensions 0.6 × 0.026 cm^2 and the power density was modulated using a series of calibrated neutral density filters. The emission from the sample was measured using a fiber coupled CCD spectrometer (Hamamatsu, Mini-spectrometer TM series, C10083CA).

ASE measurements. Randomly polarized nitrogen-gas laser (Stanford Instruments, NL-100) with emission wavelength of 337 nm and pulse width of 3.5 ns, operating at 20 Hz frequency was used to determine ASE characteristics. The laser was focused into a thin linear strip of dimension 0.5 × 0.01 cm^2 with the help of cylindrical lens and motorized slit. The samples were kept under vacuum (~10^{-5} mbar) to prevent degradation during the measurements. A set of neutral density filters were used to tune the input excitation energy. Emission was collected from the edge of the samples using an optical fiber and spectrometer (Hamamatsu, Mini-spectrometer TM series, C10083CA) with spectral resolution of 5 nm.

Data availability

The data that support the findings of this study are available from the authors upon request.

Code availability

The code used for simulations in this study is available from the authors upon request.

Received: 22 December 2020; Accepted: 28 March 2022;
Published online: 29 April 2022

References

1. Mai, V. T. N. et al. low amplified spontaneous emission threshold and efficient electroluminescence from a carbazole derivatized excited-state intramolecular proton transfer dye. *ACS Photonics* **5**, 4447–4455 (2018).
2. Shukla, A. et al. Deep-red lasing and amplified spontaneous emission from nature inspired bay-annulated indigo derivatives. *Adv. Opt. Mater.* **8**, 1901350 (2019).
3. Shukla, A. et al. Low amplified spontaneous emission and lasing thresholds from hybrids of fluorenes and vinylphenylcarbazole. *Adv. Opt. Mater.* **8**, 2000784 (2020).
4. Balijapalli, U. et al. 2,6-Dicarbonitrile diphenyl-1λ5-phosphinine (DCNP)—a robust conjugated building block for multi-functional dyes exhibiting tunable amplified spontaneous emission. *Adv. Opt. Mater.* **9**, 2101122 (2021).
5. Shukla, A. et al. Light amplification and efficient electroluminescence from a solution-processable diketopyrrolopyrrole derivative via triplet-to-singlet upconversion. *Adv. Funct. Mater.* **31**, 2009817 (2021).
6. Mai, V. T. N. et al. Lasing operation under long-pulse excitation in solution-processed organic gain medium: toward cw lasing in organic semiconductors. *Adv. Opt. Mater.* **8**, 2001234 (2020).
7. Karl, M. et al. Flexible and ultra-lightweight polymer membrane lasers. *Nat. Commun.* **9**, 1525 (2018).
8. Wang, Y. et al. LED pumped polymer laser sensor for explosives. *Laser Photonics Rev.* **7**, L71–L76 (2013).
9. Liu, X. et al. Organic semiconductor distributed feedback (DFB) laser as excitation source in Raman spectroscopy. *Opt Express* **21**, 28941–28947 (2013).

10. Clark, J. & Lanzani, G. Organic photonics for communications. *Nat. Photonics* **4**, 438–446 (2010).
11. Reilly, M. A. et al. Optical gain at 650 nm from a polymer waveguide with dye-doped cladding. *Appl. Phys. Lett.* **87**, 231116 (2005).
12. Rose, A., Zhu, Z., Madigan, C. F., Swager, T. M. & Bulović, V. Sensitivity gains in chemosensing by lasing action in organic polymers. *Nature* **434**, 876–879 (2005).
13. Sandanayaka, A. S. D. et al. Indication of current-injection lasing from an organic semiconductor. *Appl. Phys. Express* **12**, 061010 (2019).
14. Cornil, J., Beljonne, D., Calbert, J. P. & Brédas, J. L. Interchain interactions in organic π-conjugated materials: impact on electronic structure, optical response, and charge transport. *Adv. Mater.* **13**, 1053–1067 (2001).
15. Liu, J. et al. High mobility emissive organic semiconductor. *Nat. Commun.* **6**, 10032 (2015).
16. McGehee, M. D. & Heeger, A. J. Semiconducting (conjugated) polymers as materials for solid-state lasers. *Adv. Mater.* **12**, 1655–1668 (2000).
17. Coehoorn, R. Hopping mobility of charge carriers in disordered organic host-guest systems: dependence on the charge-carrier concentration. *Phys. Rev. B* **75**, 155203 (2007).
18. Aimono, T. et al. 100% fluorescence efficiency of 4,4[sup ′]-bis[(N-carbazole) styryl]biphenyl in a solid film and the very low amplified spontaneous emission threshold. *Appl. Phys. Lett.* **86**, 071110 (2005).
19. Oyama, Y. et al. Design strategy for robust organic semiconductor laser dyes. *ACS Mater. Lett.* **2**, 161–167 (2020).
20. Tang, X. et al. Color-tunable low-threshold amplified spontaneous emission from yellow to near-infrared (NIR) based on donor–spacer–acceptor–spacer–donor linear dyes. *ACS Mater. Lett.* **2**, 1567–1574 (2020).
21. Mamada, M., Komatsu, R. & Adachi, C. F8BT oligomers for organic solid-state lasers. *ACS Appl. Mater. Interfaces* **12**, 28383–28391 (2020).
22. Mamada, M., Fukunaga, T., Bencheikh, F., Sandanayaka, A. S. D. & Adachi, C. Low amplified spontaneous emission threshold from organic dyes based on bis-stilbene. *Adv. Funct. Mater.* **28**, 1802130 (2018).
23. Uoyama, H., Goushi, K., Shizu, K., Nomura, H. & Adachi, C. Highly efficient organic light-emitting diodes from delayed fluorescence. *Nature* **492**, 234–238 (2012).
24. Hasan, M. et al. Exciton–exciton annihilation in thermally activated delayed fluorescence emitter. *Adv. Funct. Mater.* **30**, 2000580 (2020).
25. Tang, X, Bai, Q., Shan, T. & Li J. Efficient nondoped blue fluorescent organic light-emitting diodes (OLEDs) with a high external quantum efficiency of 9.4% @ 1000 cd m^{-2} based on phenanthroimidazole−anthracene derivative. *Adv. Funct. Mater.* **28**, 1705813 (2018).
26. Di, D. et al. Efficient triplet exciton fusion in molecularly doped polymer light-emitting diodes. *Adv. Mater.* **29**, 1605987 (2017).
27. Hu, J.-Y. et al. Bisanthracene-based donor-acceptor-type light-emitting dopants: highly efficient deep-blue emission in organic light-emitting devices. *Adv. Funct. Mater.* **24**, 2064–2071 (2014).
28. Chiang, C.-J. et al. Ultrahigh efficiency fluorescent single and bi-layer organic light emitting diodes: the key role of triplet fusion. *Adv. Funct. Mater.* **23**, 739–746 (2013).
29. Kondakov, D. Y., Pawlik, T. D., Hatwar, T. K. & Spindler, J. P. Triplet annihilation exceeding spin statistical limit in highly efficient fluorescent organic light-emitting diodes. *J. Appl. Phys.* **106**, 124510 (2009).
30. Luo, Y. & Aziz, H. Correlation between triplet-triplet annihilation and electroluminescence efficiency in doped fluorescent organic light-emitting devices. *Adv. Funct. Mater.* **20**, 1285–1293 (2010).
31. Yokoyama, D. et al. Dual efficiency enhancement by delayed fluorescence and dipole orientation in high-efficiency fluorescent organic light-emitting diodes. *Appl. Phys. Lett.* **99**, 123303 (2011).
32. Cho, I., Kim, S. H., Kim, J. H., Park, S. & Park, S. Y. Highly efficient and stable deep-blue emitting anthracene-derived molecular glass for versatile types of non-doped OLED applications. *J. Mater. Chem.* **22**, 123–129 (2012).
33. Pu, Y. J. et al. Optimizing the charge balance of fluorescent organic light-emitting devices to achieve high external quantum efficiency beyond the conventional upper limit. *Adv. Mater.* **24**, 1765–1770 (2012).
34. Liu, W. et al. Nondoped blue fluorescent organic light-emitting diodes based on benzonitrile-anthracene derivative with 10.06% external quantum efficiency and low efficiency roll-off. *J. Mater. Chem. C* **7**, 1014–1021 (2019).
35. Ieuji, R., Goushi, K. & Adachi, C. Triplet-triplet upconversion enhanced by spin-orbit coupling in organic light-emitting diodes. *Nat. Commun.* **10**, 5283 (2019).
36. Gärtner, C., Karnutsch, C., Lemmer, U. & Pflumm, C. The influence of annihilation processes on the threshold current density of organic laser diodes. *J. Appl. Phys.* **101**, 023107 (2007).
37. Ahmad, V. et al. Charge and exciton dynamics of OLEDs under high voltage nanosecond pulse: towards injection lasing. *Nat. Commun.* **11**, 4310 (2020).
38. Bencheikh, F., Sandanayaka, A. S. D., Fukunaga, T., Matsushima, T. & Adachi, C. Origin of external quantum efficiency roll-off in 4,4′-bis[(N-carbazole) styryl]biphenyl (BSBCz)-based inverted organic light emitting diode under high pulsed electrical excitation. *J. Appl. Phys.* **126**, 185501 (2019).
39. Ullah, M., Wawrzinek, R., Maasoumi, F., Lo, S.-C. & Namdas, E. B. Semitransparent and low-voltage operating organic light-emitting field-effect transistors processed at low temperatures. *Adv. Opt. Mater.* **4**, 1022–1026 (2016).
40. Ullah, M., Wawrzinek, R., Nagiri, R. C. R., Lo, S.-C. & Namdas, E. B. UV-deep blue-visible light-emitting organic field effect transistors with high charge carrier mobilities. *Adv. Opt. Mater.* **5**, 1600973 (2017).
41. Chaudhry, M. U. et al. Nano-alignment in semiconducting polymer films: a path to achieve high current density and brightness in organic light emitting transistors. *ACS Photonics* **5**, 2137–2144 (2018).
42. Xu, Y. et al. Highly efficient blue fluorescent OLEDs based on upper level triplet-singlet intersystem crossing. *Adv. Mater.* **31**, e1807388 (2019).
43. Sharma, N. et al. Exciton efficiency beyond the spin statistical limit in organic light emitting diodes based on anthracene derivatives. *J. Mater. Chem. C* **8**, 3773–3783 (2020).
44. Qiao, X., Yuan, P., Ma, D., Ahamad, T. & Alshehri, S. M. Electrical pumped energy up-conversion: A non-linear electroluminescence process mediated by triplet-triplet annihilation. *Org. Electron.* **46**, 1–6 (2017).
45. Li, W. et al. A twisting donor-acceptor molecule with an intercrossed excited state for highly efficient, deep-blue electroluminescence. *Adv. Funct. Mater.* **22**, 2797–2803 (2012).
46. Serevičius, T. et al. Triplet–triplet annihilation in 9,10-diphenylanthracene derivatives: the role of intersystem crossing and exciton diffusion. *J. Phys. Chem. C* **121**, 8515–8524 (2017).
47. Dey, A. et al. Kinetics of thermally activated triplet fusion as a function of polymer chain packing in boosting the efficiency of organic light emitting diodes. *npj Flex. Electron.* **2**, 28 (2018).
48. Monguzzi, A., Mezyk, J., Scotognella, F., Tubino, R. & Meinardi, F. Upconversion-induced fluorescence in multicomponent systems: Steady-state excitation power threshold. *Phys. Rev. B* **78**, 195112 (2008).
49. Forget, S. & Chénais, S. in *Organic Solid-State Lasers* (eds. Forget, S. & Chénais, S.) 13–73 (Springer, 2013).
50. Michel-Beyerle, M. E., Haberkorn, R., Kinder, J. & Seidlitz, H. Direct evidence for the singlet-triplet exciton annihilation in anthracene crystals. *Phys. Status Solidi B* **85**, 45–49 (1978).
51. Zhang, Y. & Forrest, S. R. Triplets contribute to both an increase and loss in fluorescent yield in organic light emitting diodes. *Phys. Rev. Lett.* **108**, 267404 (2012).
52. Dey, A., Rao, A. & Kabra, D. A Complete quantitative analysis of spatio-temporal dynamics of excitons in functional organic light-emitting diodes. *Adv. Opt. Mater.* **5**, 1600678 (2017).
53. Wallikewitz, B. H., Kabra, D., Gélinas, S. & Friend, R. H. Triplet dynamics in fluorescent polymer light-emitting diodes. *Phys.Rev. B* **85**, 045209 (2012).
54. Dey, A. & Kabra, D. Role of bimolecular exciton kinetics in controlling the efficiency of organic light-emitting diodes. *ACS Appl. Mater. Interfaces* **10**, 38287–38293 (2018).
55. Karunathilaka, B. S. B. et al. Suppression of external quantum efficiency rolloff in organic light emitting diodes by scavenging triplet excitons. *Nat. Commun.* **11**, 4926 (2020).
56. Nakanotani, H., Furukawa, T. & Adachi, C. Light amplification in an organic solid-state film with the aid of triplet-to-singlet upconversion. *Adv. Opt. Mater.* **3**, 1381–1388 (2015).
57. Grede, A. J. & Giebink, N. C. Lasing in the space charge limited current regime. *Phys. Rev. B* **103**, L121301 (2021).
58. Yoshida, K., Nakanotani, H. & Adachi, C. Effect of Joule heating on transient current and electroluminescence in p-i-n organic light-emitting diodes under pulsed voltage operation. *Org. Electron.* **31**, 287–294 (2016).
59. Hasan, M. et al. Probing polaron-induced exciton quenching in TADF based organic light-emitting diodes. *Nat. Commun.* **13**, 254 (2022).

Acknowledgements

The authors thank Department of Industry, Innovation and Science (AISRF53765) and Australian Research Council (DP160100700 and DP200103036) for funding this work. A.S. was supported by UQ's Research and Training Program, M.H. and V.A. were funded by Australian Postgraduate Award (APA). This work was performed in part at the Queensland node of the Australian National Fabrication Facility Queensland Node (ANFF-Q), a company established under the National Collaborative Research Infrastructure Strategy to provide nano- and microfabrication facilities for Australia's researchers. DK acknowledges DST-AISRF (No. DST/INT/AUS/P-74/2017) for funding support.

Author contributions

A. S., S.-C.L., and E.B.N. conceived the idea of the manuscript. A.S., V.A., G.S.B., performed the experiments and analyzed the results with the help of J.S. Theoretical model was developed by M.H. and A.S. under the guidance of E.B.N. M.H. fitted the experimental data with the full model and generated the simulated results. A.S. drafted the

manuscript. E.G.M., D.K., S.-C.L., and E.B.N. supervised the work. All the authors contributed to data analysis and discussion of the results.

Competing interests

The authors declare no competing interests.

Additional information

Supplementary information The online version contains supplementary material available at https://doi.org/10.1038/s43246-022-00248-0.

Correspondence and requests for materials should be addressed to Atul Shukla ,Dinesh Kabra ,Shih-Chun Lo or Ebinazar B. Namdas.

Peer review information *Communications Materials* thanks the anonymous reviewers for their contribution to the peer review of this work. Primary Handling Editor: John Plummer. Peer reviewer reports are available.

Reprints and permission information is available at http://www.nature.com/reprints

Publisher's note Springer Nature remains neutral with regard to jurisdictional claims in published maps and institutional affiliations.

Open Access This article is licensed under a Creative Commons Attribution 4.0 International License, which permits use, sharing, adaptation, distribution and reproduction in any medium or format, as long as you give appropriate credit to the original author(s) and the source, provide a link to the Creative Commons license, and indicate if changes were made. The images or other third party material in this article are included in the article's Creative Commons license, unless indicated otherwise in a credit line to the material. If material is not included in the article's Creative Commons license and your intended use is not permitted by statutory regulation or exceeds the permitted use, you will need to obtain permission directly from the copyright holder. To view a copy of this license, visit http://creativecommons.org/licenses/by/4.0/.

© The Author(s) 2022